A Pd/Monolayer Titanate Nanosheet with Surface Synergetic Effects for Precise Synthesis of Cyclohexanones

Yujie Song,[†] Hao Wang,[†] Xiaomei Gao,[†] Yingxin Feng,[†] Shijing Liang,*[,†,‡] Jinhong Bi,[†,‡] Sen Lin,*[,†] Xianzhi Fu,[†] and Ling Wu*[,†]

[†]State Key Laboratory of Photocatalysis on Energy and Environment and [‡]Department of Environmental Science and Engineering, Fuzhou University, Fuzhou 350116, P. R. China

S Supporting Information

ABSTRACT: A catalyst composed of monolayer nonstoichiometric titanate nanosheets (denoted as TN) and Pd clusters is constructed for precise synthesis of cyclohexanone from phenol hydrogenation with high conversion (>99%) and selectivity (>99%) in aqueous media under light irradiation. Experimental and DFT calculation results reveal that the surface exposed acid and basic sites on TN could interact with phenol molecules in a nonplanar fashion via a hexahydroxy hydrogen-bonding ring to form a surface coordination species. This greatly facilitates the adsorption and activation of phenol molecules and suppresses the further hydrogenation of cyclohexanone. Moreover, the surface Pd clusters serve as the active sites for the adsorption and dissociation of hydrogen molecules to provide active H atoms. The synergistic effect of the surface coordination species, TN and Pd clusters remarkably facilitate the high yield of cyclohexanone in photocatalysis. Finally, the possible thermo/photocatalytic mechanisms on Pd/TN are proposed. This work not only highlights the great potential for monolayer nonstoichiometric composition nanosheets in the construction of catalysts for precise organic synthesis but also provides insight into the inherent catalytic behavior at a molecular level.

KEYWORDS: monolayer titanate nanosheet, hydrogenation of phenol, precision synthesis, green photocatalysis
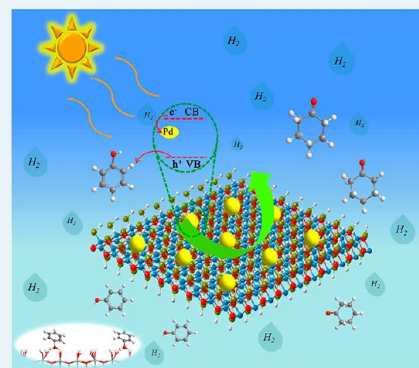
1. INTRODUCTION

As a key chemical intermediate, cyclohexanone can be used as precursor for the production of caprolactam for nylon-6 and adipic acid for nylon-66.[1−4] Traditionally, cyclohexanone is produced on a commercial scale either by the oxidation of cyclohexane or hydrogenation of phenol. The oxidation of cyclohexane is far from satisfactory because of harsh reaction conditions.[5] This reaction has also suffered from low product yields. An attractive route for the production of cyclohexanone is selective hydrogenation of phenol in liquid phase by a one-step process because the catalytic system offers atom-efficiency and cost/energy savings.[6,7] It was found that phenol hydrogenation could be catalyzed efficiently by Pd catalysts. Numerous Pd catalytic systems have been developed such as Pd/C, Pd/MgO, Pd/Al$_2$O$_3$, Pd/mesoporous silica, Pt/H-ZSM-5, and Pd/MOFs (such as MIL-101 and MIL-53).[8−11] However, these catalytic systems need high temperature, high H$_2$ pressure, and toxic regents. Han et al. introduced Lewis acid AlCl$_3$ into the Pd/C catalysis system to achieve the excellent conversion of phenol hydrogenation.[12] The additives such as AlCl$_3$ may restrict the application of these hosts in the hydrogenation reaction and against the product purity and reaction conditions. So far, despite a lot of work on phenol hydrogenation, these works mainly focused on the thermocatalysis and the search for suitable Lewis acid additives. More importantly, the heterogeneous catalytic mechanism of phenol

hydrogenation is still unclarified at the molecular level. Therefore, developing a versatile green and new approach for selective hydrogenation of phenol is desirable. Additionally, a comprehensive understanding of the catalytic process is still a huge challenge, but it has great promise in potential applications.

The surface properties of supports are one of the most important factors in selective hydrogenation of phenol. More Lewis acid sites on the catalysts could enhance the chemisorption of phenol and promote the conversion rate of phenol hydrogenation, while the selectivity of cyclohexanone may be suppressed.[13−15] More basic sites would improve the selectivity toward cyclohexanone, but the transformation efficiency of phenol may be restricted.[16−18] Therefore, it is essential to construct a versatile catalyst with the appropriate acid−basic sites for the precise synthesis of cyclohexanone in high yield under a mild and eco-friendly condition.

Recently, two-dimensional (2D) oxide nanosheets have attracted great attention in many fields.[19−22] In our previous work, niobate nanosheets with abundant surface acid sites showed higher photocatalytic activities for benzyl alcohols than their layered counterparts because of their ultrathin structure
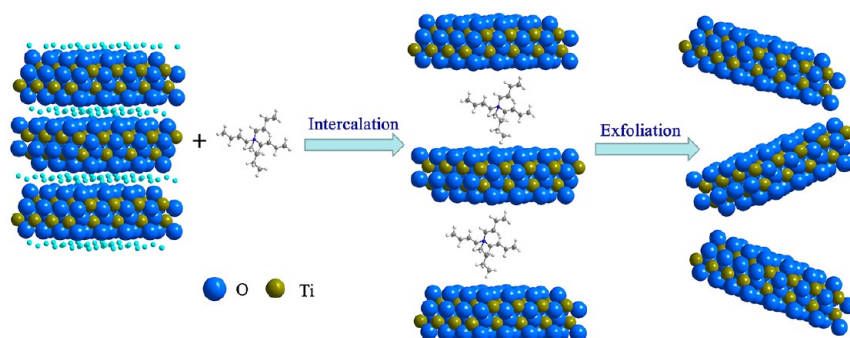
Figure 1. Exfoliation process of layered $H_{1.07}Ti_{1.73}O_4 \cdot H_2O$ into $H_{1.07}Ti_{1.73}O_4 \cdot H_2O$ nanosheets.
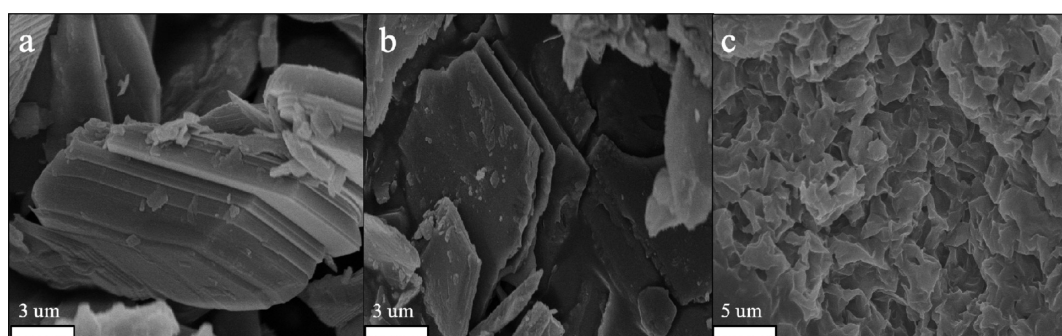

Figure 2. SEM images for layered $K_{0.8}Ti_{1.73}Li_{0.67}O_4$ (a), LT (b), and TN (c).
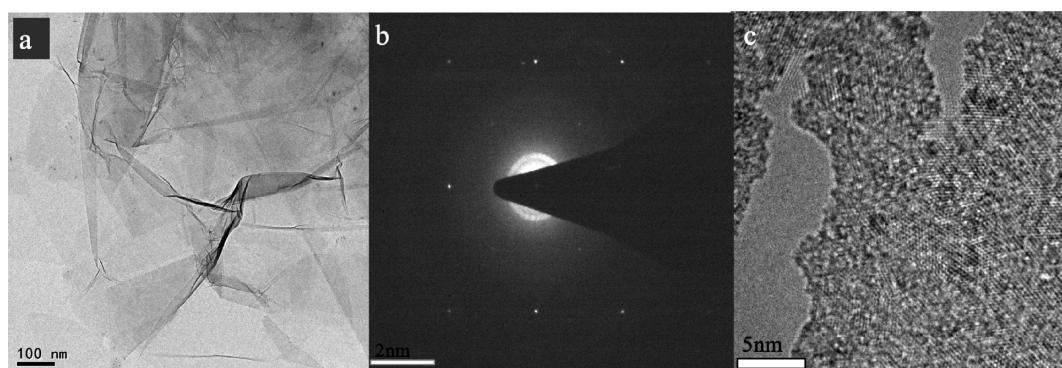

Figure 3. TEM (a), SAED pattern (b), HRTEM (c) images of TN.

with high external surface area and an extremely high percentage of surface atoms.[23−28] Similarly, the Lepidocrocite titanates nanosheets (denoted as TN): $H_{1.07}Ti_{1.73}O_4 \cdot H_2O$, has an orthorhombic structure consisting of two species oxygen atoms: the 2-coordinated oxygen ($\mu2$-O, denoted as O1) and 4-coordinated oxygen ($\mu4$-O, denoted as O2)[29−31] The abundant Ti defects may lead to unsaturated O2 atoms that serve as the weak Lewis base sites. The O1 atoms shared by two nearby Ti^{4+} provide strong Lewis base sites. The H^+ bonded with an O1 atom acts as a strong Brønsted acid sites. Furthermore, the exposed Ti^{4+} ions act as Lewis acid sites. Therefore, the TN with abundant surface acid and base sites may be an ideal material to construct a catalyst for the precise synthesis of cyclohexanone.

Herein, on the basis of the characterizations for TN and the adsorption behaviors of phenol molecules, we designed a catalyst for the precise synthesis of cyclohexanone. It is composed of Pd clusters (∼3 nm) and monolayer $H_{1.07}Ti_{1.73}O_4 \cdot H_2O$ nanosheets (denoted as Pd/TN). The catalyst exhibits high phenol conversion (>99%) and high cyclohexanone selectivity (>99%) under ambient temperature and hydrogen atmosphere using water as solvent. It is much better than the layered counterparts. The surface properties and interaction with phenol molecules on the catalyst were investigated by in situ molecular spectroscopic techniques and theoretical DFT calculations. The photopromoted surface catalytic reaction process was discussed on the basis of the experimental results. Finally, a probable photopromoted surface synergetic catalytic mechanism has been revealed at a molecular level.

2. RESULTS AND DISCUSSION

The TN sample was prepared by a cation-exchange/exfoliation process similar to a previous report using layered $K_{0.8}Ti_{1.73}Li_{0.67}O_4$ as the precursor (Figure 1).[29] The XRD patterns confirm that the layered $K_{0.8}Ti_{1.73}Li_{0.67}O_4$, the layered $H_{1.07}Ti_{1.73}O_4 \cdot H_2O$ (LT) and TN with pure phase have been prepared (Figure S1). After a proton-exchange process, the characteristic peak (020) shifted to a lower 2θ angle suggesting
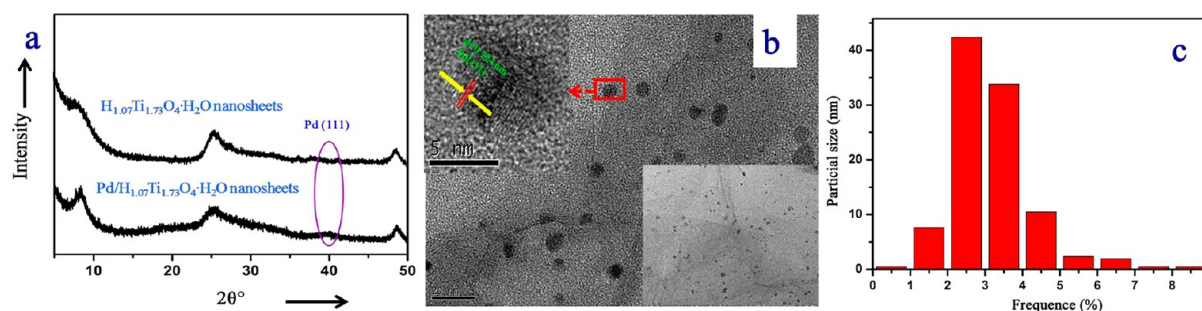
Figure 4. (a) XRD patterns of TN and Pd/TN; (b) TEM and HRTEM of Pd/TN; (c) Size distribution of Pd clusters on TN.

a distensible interlayer distance of 0.72 nm for $K_{0.8}Ti_{1.73}Li_{0.67}O_4$ to 0.89 nm for LT. This swelling process is beneficial to the intercalation-exfoliation process for the formation of TN. After exfoliation, the disappearance of the characteristic peak (020) of TN indicates the loss of the periodic layered structure of LT.[26]

SEM images show that the $K_{0.8}Ti_{1.73}Li_{0.67}O_4$ and LT have a typical layered structure stacked layer-by-layer (Figure 2a,b); the as-prepared TN sample shows a loose and lamellar structure (Figure 2c). The TEM images of TN further confirm the morphologies of the tissue-like ultrathin 2D nanosheets (Figure 3). These results agree well with the XRD results. The selected-area electron diffraction (SAED) pattern shows the single crystalline nature of the ultrathin layer TN. The clear lattice fringes demonstrate that these nanosheets retain their high crystallinity. The AFM image shows that the thickness of the TN is about 1.1 nm, suggesting that the as-prepared TN sample is only one monolayer thick (1 nm) (Figure S2).[32] This confirmed that the monolayer TN sample was successfully prepared. The photoabsorption performances of the samples have been analyzed by UV−vis DRS (Figure S3). It is obvious that the photoabsorption performance of TN is much higher than that of LT. This may be due to the large photoabsorption area and the surface electron structure of the 2D nanosheets.

The Pd/TN samples were synthesized by a photoreduction process. The Pd/TN shows a very similar XRD pattern with the parent TN, indicating that the loading of Pd clusters has a negligible influence on the crystal structure of TN (Figure 4). A characteristic peak at 40.0° assigned to the (111) crystal planes of Pd clusters can be clearly observed indicating the formation of Pd clusters on the TN. Certainly, the prepared Pd/TN powders were easily aggregated after they were collected and dried at 60 °C (Figure S4a). Because of the electrostatic repulsion of the polyanion layers and the sustaining of Pd clusters, these restacked nanosheets have a large distance between the two layers. Thus, the obtained Pd/TN powder is easy to redisperse into the monolayer nanosheet in water (Figure S4b). As shown in Figure 4b, the restacked Pd/TN has dispersed into ultrathin nanosheets. The Pd clusters with the mean sizes of 3 nm are well-dispersed on the surface of the ultrathin nanosheets. HRTEM shows that the lattice fringe of 0.224 nm matches the interplanar spacing of the (111) planes of metallic Pd.[33] The loading concentration of Pd in Pd/TN was determined to be 2 mol % by ICP-OES.

The surface properties of TN are further studied in detail. From the crystal structure of TN, we expect strong superficial acidity and basicity on TN (Figure 5). These superficial properties are investigated by in situ FTIR spectra of pyridine adsorption. Figure 6 shows that pyridine is adsorbed on TN. The strong peaks located at 1485 and 1540 cm^{-1} are attributed
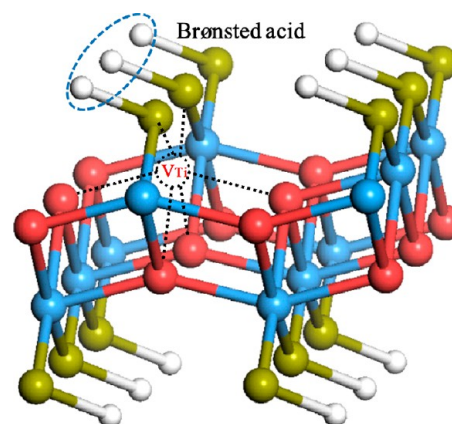

Figure 5. Schematic structure of $H_{1.07}Ti_{1.73}O_4 \cdot H_2O$ nanosheets. Atoms are color labeled: Ti (blue), H (white), O1 (red), and O2 (green).

to pyridine on the strong Brønsted acid sites. Furthermore, a strong and sharp peak at 1450 cm^{-1} is observed, which is assigned to pyridine on the Lewis acid.[26] These peaks remain even after subsequent evacuation indicating the chemisorption of pyridine and the strong acidity in the surface of TN. However, there is no noticeable peak over the LT sample. It should be noted that the LT and TN have the same amount of the acidic sites per unit mass. The preparation method of TN, an intercalation-exfoliation process from the parent LT, makes the sites exposed. Because of the very small distance between two adjacent layers in LT, the adsorption of pyridine molecules on the interlayer acidic sites would be restricted. Thus, the in situ pyridine-adsorbed FTIR showed that the amount of acidic sites exposed on the surface of LT is much lower than that on TN.[35] Therefore, the amount of Brønsted acid and Lewis acid sites exposed on the surface of LT is much lower than that on TN, and the surface acidity of LT is very weak. These results also confirm the presence of acid sites in the titanate sample, and they are greatly enhanced when it is prepared into a 2D nanosheet.

Next, we performed the solid-state ^{1}H NMR spectroscopy to gain more insights into the properties of hydrogen species on TN. Figure 7 shows the ^{1}H NMR for TN before and after dehydration. Before the dehydration, three peaks are observed at the chemical shift values of about 10.3, 6.3, and 1.3 ppm. These are assigned to the strong acidic OH groups, H_3O^+ species, and the isolated Ti−OH, respectively. After dehydration, the peaks at 10.2, 7.4, 4.6, and 1.3 ppm are assigned to the strong acidic OH groups, Ti (OH) Ti, Ti−OH with hydrogen-bonds, and Ti−OH groups without hydrogen bonds, respectively. The Ti (OH) Ti of bridging hydroxyl groups may function as the strong Brønsted acid sites.[36,37]
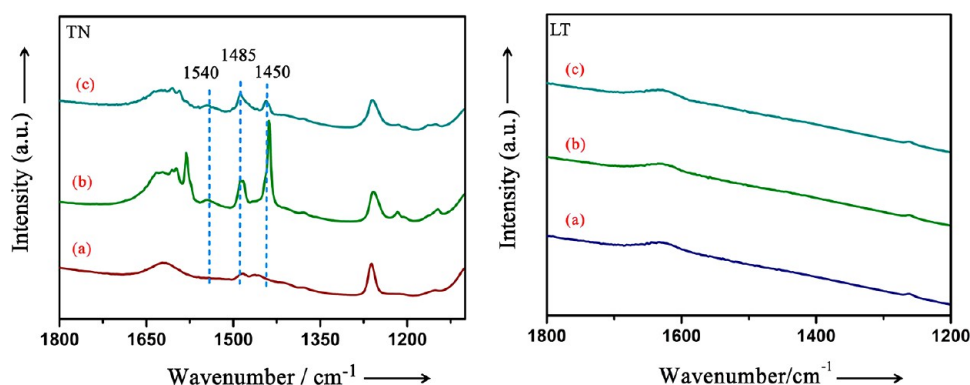
Figure 6. In situ FTIR spectra of the TN and LT for pyridine-adsorbed sample. (a) After degassing at 150 °C for 4 h. (b) Adsorption for 30 min at RT (physisorption+chemisorption). (c) Further evacuation of excess probe molecules at 150 °C for 5 min (chemisorption).
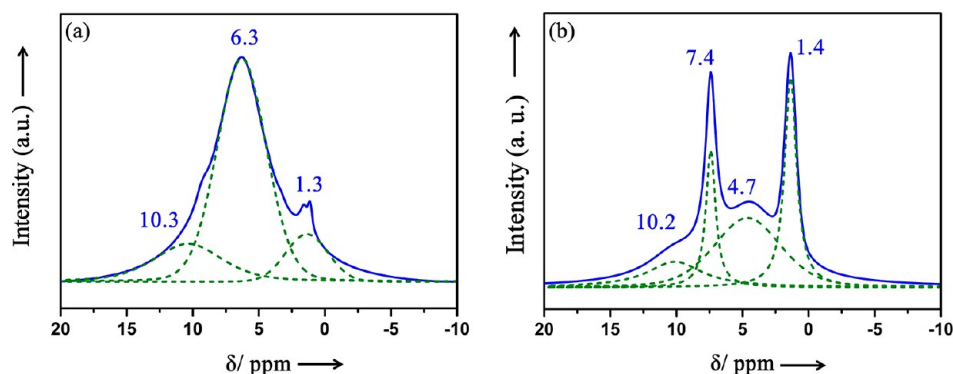

Figure 7. ^1H magic angle spinning NMR spectra for TN before (a) and after dehydration (b).

The surface basicity of TN and LT were determined by CO_2-TPD experiments (as shown in Figure 8). The TN sample
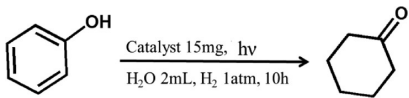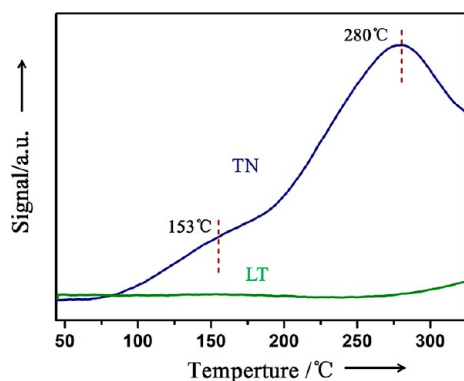

Figure 8. Temperature-programmed desorption profiles of TN and LT.

clearly adsorbed abundant CO_2 molecules via the chemisorption, but there is no distinct adsorption of CO_2 on LT. These results demonstrate that the superficial basicity of TN is much higher than that of LT, which may be resulted by the unique structural features of TN. The 2D configuration provides an extremely high percentage of superficial exposed unsaturated atoms. The CO_2 molecules could not adsorb on the interlayer of the LT because of the steric inhibition of the adjacent layers. This would result in the low concentration of basic sites. Moreover, the BET specific surface area of TN is about 176.2 $m^2 g^{-1}$, which is about 21.5 times larger than that of LT (8.2 $m^2 g^{-1}$) (Figure S5). This occurs because the interlayered

confinement effect in LT has been overcome efficiently for TN. Thus, the measured surface area of TN is much higher than that of LT. Furthermore, the steric inhibition effect also limits the utilization of the active sites on the interlayer of LT, although the concentration of the active sites of LT may be similar to that of TN. The high number of the exposed active sites could absorb more phenol molecules to enhance the mass transfer. The photocatalytic activity would also be increased. Additionally, the CO_2-TPD curve of TN shows two obvious desorption peaks at about 153 and 280 °C. The former peak may be ascribed to desorption of CO_2 adsorbed on the weak basic sites of TN. The latter one may be ascribed to desorption of CO_2 adsorbed on the strong basic sites of TN. It is worth noting that the CO_2 desorption peak area of the strong basic sites is much higher than the weak basic sites. That is, the concentration of the strong basic sites is much higher than that of the weak basic sites. When combined with the crystal structure of TN, it is possible that the weak basic site may be the O2 atoms shared by for Ti atoms and that the strong basic site may be the surface unsaturated O1 atoms of TN.

It has been generally accepted that the surface properties have tremendous effects on the catalytic properties of the nanomaterials. Thus, to understand the effect of the distinctive surface structure of TN on the catalytic performance, the photocatalytic hydrogenation of phenol to cyclohexanone was carried out over the samples under the simulated solar light (750 nm $\geq \lambda \geq$ 300 nm) irradiation at 298 K with hydrogen atmosphere using water as the solvent (Table 1). The thermostat bath was used to control the given temperature (Figure S6). An almost quantitative transformation of phenol (>99%) with high yield (>99%) to cyclohexanone is achieved

Table 1. Hydrogenation of Phenol Molecules over the Samples with and without Stimulated Irradiation[a]

Catalyst 15mg, hν
H$_2$O 2mL, H$_2$ 1atm, 10h

entry	catalyst	hν	temp (K)	conv. (%)	C=O (%)	C–O (%)
1	Pd/TN	+	298	>99	>99	<1
2	Pd/TN	–	298	21	>99	<1
3	Pd/TN	–	333	51	99	1
4	-	+	298	0	0	0
5	TN	+	298	0	0	0
6	Pd/LT	+	298	15	>99	<1
7	Pd/LT	-	298	10	>99	<1

[a]Reaction conditions: simulated sunlight (750 nm ≥ λ ≥ 300 nm), phenol (0.1 mmol), catalyst (15 mg, 2 mol % Pd,), water (2 mL), H$_2$ (1 atm) unless otherwise noted.

over the Pd/TN under irradiating for 10 h. No byproducts such as cyclohexanol and cyclohexane were detected, indicating that the precise synthesis of cyclohexanone can be realized over the Pd/TN. It is worth mentioning that the experiment can be scaled up without an obvious decrease in performance. Efficient conversion of phenol (>92%) is observed with high selectivity to cyclohexanone (>99%) over Pd/TN under simulated solar light irradiation for 10 h when the concentration of phenol is scaled up by a factor of 10. Furthermore, the catalytic activities are negligible in the absence of Pd/TN or Pd clusters. In addition, when the reactions are carried out in the dark, only 21% of the phenol is catalyzed to cyclohexanone at 298 K. When the reaction temperature increased to 333 K, the phenol conversion can increase to 51% in the dark. These results reveal that the hydrogenation of phenol is driven by Pd clusters with the assistance of TN, and the catalytic activities of Pd/TN can be greatly enhanced under the simulated solar light irradiations. Thus, the Pd/TN composite would make full use of the thermal and light energy to more efficiently drive the phenol hydrogenation reaction at room temperature. The reusability and stability of the catalyst are also studied (Figure S7 and S8). The recycling of the catalyst for four runs shows no obvious decrease of catalytic activity. After the reaction, the separation of the catalyst from the heterocatalytic system is very facile, and the catalyst can be reused directly. The XRD patterns and XPS spectra of Pd/TN are almost unchanged after the photo-

catalytic reactions, demonstrating the high stability of the Pd/TN photocatalyst (Figure S8).

To elucidate the role of TN, a set of controlled experiments were performed (Table S1). Because TN could not be excited by visible light (Figure S3), a greatly decreased photocatalytic activity is obtained over the Pd/TN under the visible light irradiation (750 nm ≥ λ ≥ 420 nm, 25% conv.), suggesting that the photoexcited TN can efficiently facilitate the transformation of phenol. Compared with Pd/TN, it is obvious that the Pd/LT sample exhibits a much lower conversion rate with or without light irradiation (Table 1, entries 6, 7). Moreover, when the common photocatalyst anatase TiO$_2$ used as a support (Table S1, entries 2, 3), Pd/anatase TiO$_2$ shows the much lower photocatalytic activities (<2% Conv. in the dark and 5% Conv. under the visible light irradiation) than those of Pd/TN (21% conv. and 25% conv., respectively, Table S1, entry 1). In addition, negligible cyclohexanone is observed, when the Pd/Al$_2$O$_3$ as a catalyst at 1 atm H$_2$ under the room temperature or visible light irradiation (Table S1, entries 4−6). For a better comparison of the TN and Al$_2$O$_3$-supported catalyst, we have carried out the TEM images of the Pd/Al$_2$O$_3$ sample for the characterization of Pd clusters (Figure S9). It can be observed that the average size of the Pd clusters on the Al$_2$O$_3$ is 3 nm, similar to that on the TN. Moreover, the XPS spectra for Pd/Al$_2$O$_3$ were also characterized to examine the surface chemical state of Pd clusters. As shown in Figure S10a, the 334.9 and 340.2 eV are assigned for the Pd 3d$_{5/2}$ and Pd 3d$_{3/2}$ of Pd^0, respectively.[1,8,9] The spectra of Pd 3d suggest that Pd clusters are in a metallic form on the Al$_2$O$_3$. The difference in activities between Pd/TN and Pd/Al$_2$O$_3$ could be attributed to the distinctive properties of the supports. Therefore, it is reasonable to deduce that the phenol molecules can directly interact with the TN for the further activation and transformation. The enhanced catalytic activity may be attributed to the distinctive surface structure and unique electronic properties of 2D titanate nanosheets.[34]

The interaction between TN and the phenol molecules was revealed by in situ FTIR spectroscopy (Figure 9A). It is obvious that phenol molecules could chemisorb on the surface of TN even with the evacuation at 150 °C. Three peaks at about 1620, 1495, and 1250 cm^{-1} was observed. These peaks can be assigned to the σ(C=C) and σ(C–O), respectively.[38] However, the cyclohexanone molecules can only physisorb on the surface of TN (Figure 9B), resulting in the easy released
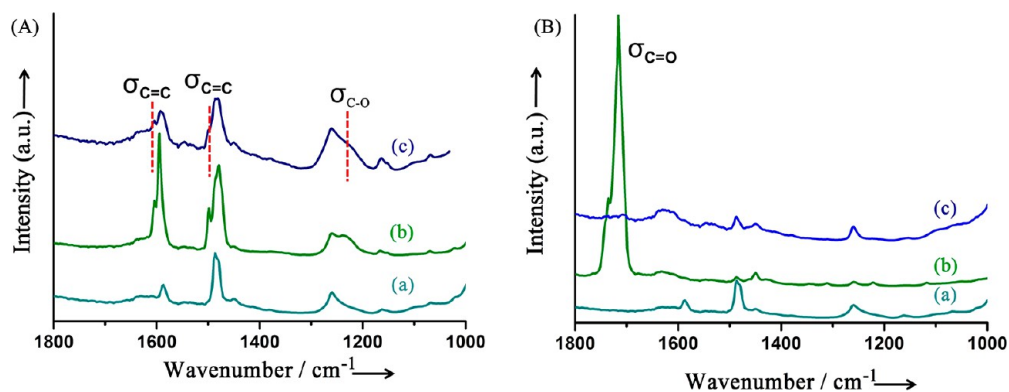

Figure 9. In situ FTIR spectra of the monolayer TN for phenol (a) and cyclohexanone adsorbed (b). (a) After degassing at 150 °C for 4 h. (b) Adsorption for 30 min at RT (physisorption+chemisorption). (c) Further evacuation of excess probe molecules at 150 °C for 5 min (chemisorption).
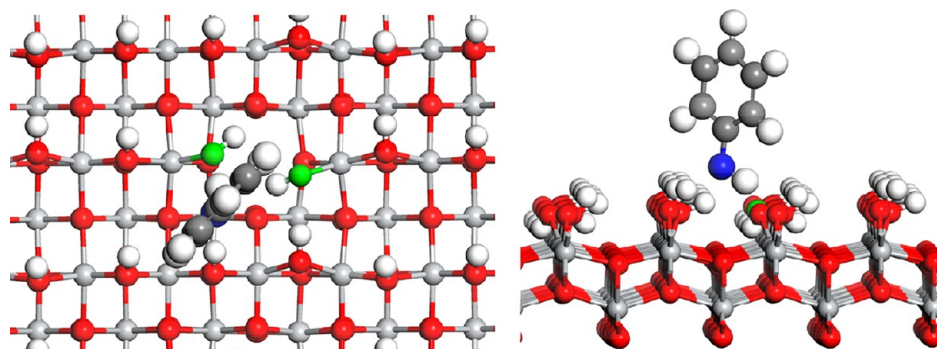
Figure 10. Top view (left) and side (right) of the most stable adsorption configuration of phenol. Atoms are color labeled: Ti (light gray), H (white), C (gray), O atoms (red) in TN, O atoms (blue) in phenol and O (green) atoms interacted with the phenol molecule.
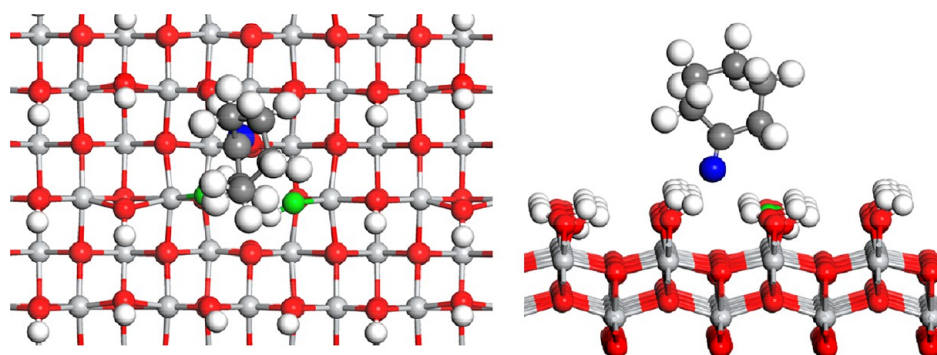

Figure 11. Top view (left) and side (right) of the most stable adsorption configuration of cyclohexanone. Atoms are color labeled: Ti (light gray), H (white), C (gray), O atoms (red) in TN, O atoms (blue) in cyclohexanone and O atoms (green) interacted with the cyclohexanone molecule.

products from the catalyst. Moreover, the adsorption sites were further revealed by theoretical density functional theory (DFT) calculations. As shown in Figures 10 and 11, the results suggest that the phenol molecules anchor on the surface of TN by the strong Ar−OH···O2 and Ar−O···HO2 interactions via a hydrogen-bonding ring (Figure 10) forming the surface coordination species.[36] The adsorption energy of phenol and cyclohexanone molecules on TN in a stable adsorption configuration is estimated to be 1.25 eV. However, the adsorption energy of cyclohexanone is only 0.91 eV. These results agree with that of in situ FTIR. The strong chemisorption of phenol molecules on TN with a surface coordination species could facilitate the activation and transformation of phenol molecules.[39] Additionally, the easy desorption of cyclohexanone in the surface active sites could efficiently inhibit the over hydrogenation of cyclohexanone. Thus, the hydrogenation of phenol would be catalyzed at a high conversion rate with the high selectivity that we observed.

To find out where the reaction takes place exactly, the adsorption of phenol molecules on the Pd clusters should be also calculated via the theoretical density functional theory (DFT) calculations. Minimum size of Pd clusters is about 0.6 nm characterized by TEM images (Figure 4) in this work. Thus, the Pd_{13} with a similar size was selected as a catalyst model for the phenol adsorption. The adsorption energies of phenol on the Pd_{13} cluster/TN interface and pure Pd_{13} cluster were calculated and then compared with the value on TN. As shown in Figure 12, the adsorption energies of phenol on Pd_{13} cluster/TN interface and pure Pd_{13} cluster are about 0.89 and 0.93 eV, respectively. For phenol on the TN, the adsorption energy is 1.25 eV, suggesting that the phenol molecules prefer to adsorb on the TN. These results are in good agreement with
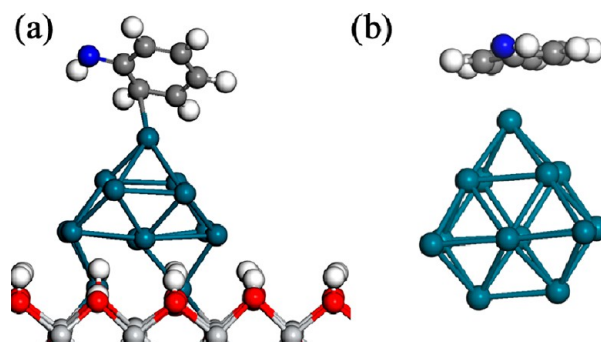

Figure 12. Optimized structures of the adsorption of phenol on Pd_{13}/TN (a) and pure Pd_{13} (b). Atoms are color labeled: Ti (light gray), H (white), O (red), and C (gray), O atom (blue) in phenol and cyclohexanone, Pd (grayish blue).

the in situ FTIR for phenol adsorption on the TN. The phenol molecules would adsorb on the TN via the formation of surface coordination species, resulting in the activation of phenol molecules. This reduces the potential energy of phenol to cyclohexanone, increasing the catalytic transformation of phenol molecules. Moreover, a set of control experiments also suggested that the conversion efficiency of phenol depends enormously on the supports of Pd clusters. Therefore, the roles of Pd clusters are not responsible for the adsorption of phenol molecules. However, the Pd clusters are indispensable for the phenol hydrogenation because negligible cyclohexanone was obtained in the absence of Pd clusters. Thus, the Pd clusters could be the main active sites for the dissociation of H_2 to H atoms as reported in the literature.[12,13,40] Moreover, the hydro-oxygen titration for Pd/TN and TN was carried out to further
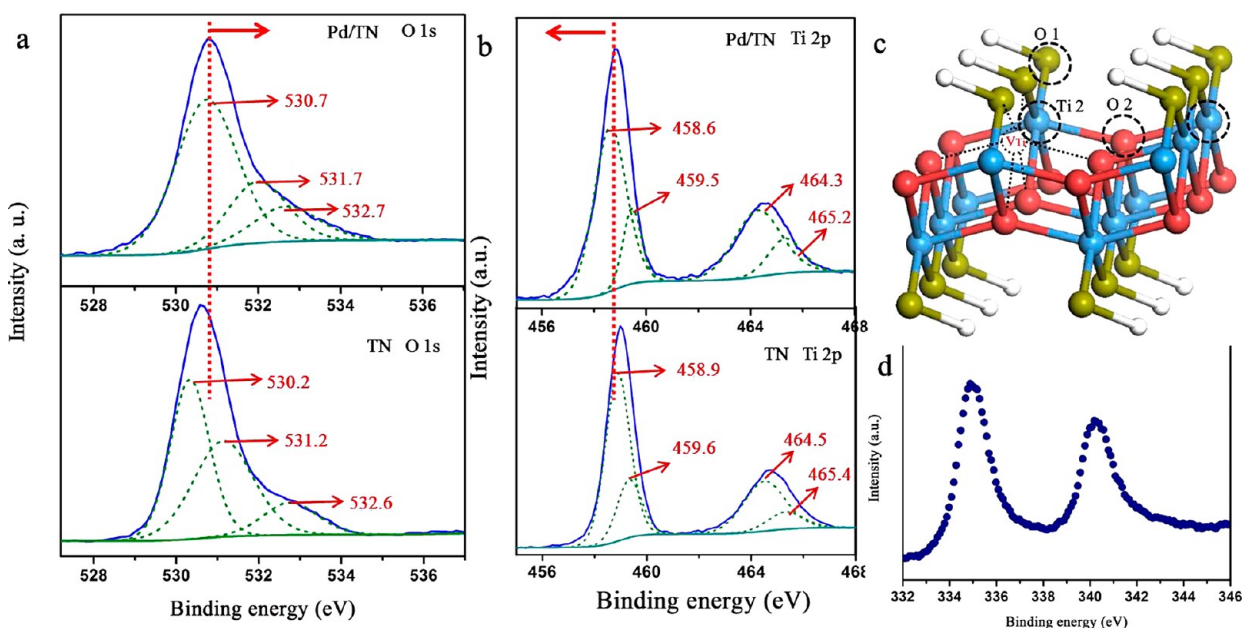
Figure 13. XPS spectra of O 1s (a), Ti 2p (b) for TN and Pd/TN. The structure of TN (c) and the XPS spectrum of Pd 3d for surface Pd clusters.

elucidate the dissociation of H_2 molecules on Pd clusters. Figure S12 shows the obvious signal of H_2O at 60 °C over Pd/TN. Meanwhile, a later peak is observed at 275 °C over Pd/TN sample, which is attributed to the dissociative adsorption of hydrogen on Pd clusters.[41] However, TN exhibits no obvious signals for H_2O and dissociation of hydrogen, indicating that the TN cannot adsorb and activate the H_2 molecules. Therefore, the Pd clusters are the main active site for the dissociation of H_2 to activate H atoms.

Considering that the phenol hydrogenation could be performed with a relatively high activity over the Pd/TN in the dark and no catalytic activity over TN, Pd clusters play a key role in the catalytic reactions. The surface chemical states of Pd, O, and Ti elements on Pd/TN were disclosed by X-ray photoelectron spectroscopy (XPS). Figure 13 shows the high resolution XPS spectra of O 1s, Ti 2p and Pd 3d for TN and Pd/TN. The curve of O 1s on TN are deconvoluted into three peaks at about 530.2, 531.2, and 532.6 eV assigned to the O1, O2 and absorbed oxygen species, respectively.[28−31] The Ti 2p spectrum of TN can be deconvoluted into two peaks at 458.9 and 459.6 eV for Ti $2p_{3/2}$, representing two type of Ti species (Figure 13b). The former Ti species (Ti1) is origin from the perfect octahedral TiO_6 and the latter (Ti2) is attributed to the Ti species nearby the Ti vacancies (Figure 13c). It is obvious that the binding energies of O1 and O2 are shifted to the higher values, and the binding energy of Ti1 is shifted to the lower value after the Pd loaded on the TN via an in situ photoreduction method. Moreover, The curve of Pd 3d is fitted into two peaks at 335.2 and 340.4 eV for Pd $3d_{5/2}$ and Pd $3d_{3/2}$, respectively, suggesting that the loaded Pd is metallic Pd^0 (Figure 13d).[1,8,9,42] These results also suggest that the surface Pd clusters are locate at the perfect octahedral TiO_6 via the electrons transfer from lattice oxygen to Ti1 and further to the surface adsorbed Pd^{2+} ions under the simulated solar light irradiation.

How do the surface coordination species facilitate the activation and transformation of phenol molecules? The in situ electron spin resonance (ESR) and diffuse reflectance UV−visible spectroscopy (UV−vis DRS) techniques were used to

reveal the role of the surface coordination species in phenol hydrogenation. The in situ ESR spectroscopy (Figures 14 and
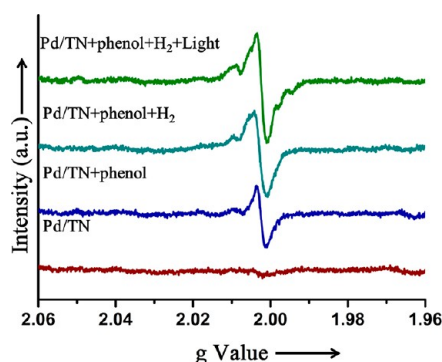

Figure 14. ESR spectra of Pd/TN.

15) was carried out to elucidate the changes of electron structures in surface catalytic reaction. Neither Pd/TN nor Pd/LT initial catalysts show ESR signals. However, when phenol molecules adsorbed on the surface of catalyst, an obvious ESR signal of oxygen vacancies (V_O, g = 2.003) could be observed, and this is further enhanced under the light irradiation. Moreover, as shown in Figure 15a, V_O is also produced when the phenol molecule is adsorbed on the monolayer TN, although the intensity is weaker than that on Pd/TN. This result suggests that V_O derives from the chemical interaction between phenol and monolayer TN. The surface coordination species can induce the formation of V_O by the surface charge distribution. Combining with the crystal structure of $H_{1.07}Ti_{1.73}O_4 \cdot H_2O$, the existence of Ti defects may induce the transformation of superficial O1 atoms into the terminal oxygen atoms (denoted as T-O). Because of the strong chemical adsorption for phenol molecules (Figure 14) as well as the influence of adjacent Pd clusters, this T-O atom may be removed from the initial position to form V_O. Furthermore, the resulting V_O may cause the exposition of intimal Ti^{4+} and the adsorbed phenol molecules might interact with these Ti^{4+} in a
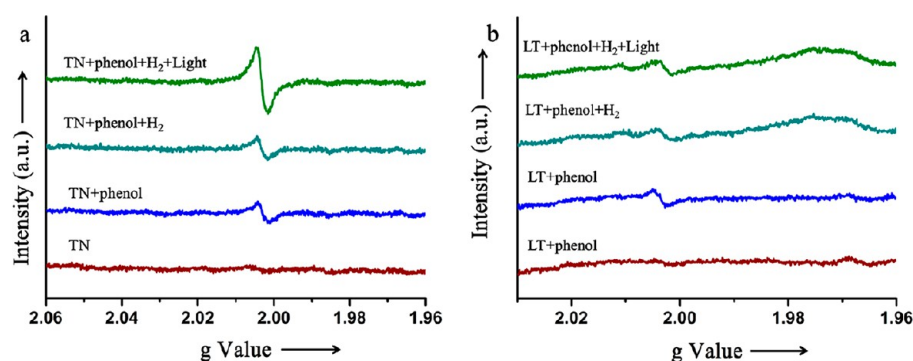
Figure 15. ESR spectra of TN (a) and LT (b).

nonplanar fashion. Moreover, the adjacent deposited Pd clusters can enhance the concentration of V_O. The intensity of the ESR signal for TN is much higher than that for LT (Figure 15b) because of the higher percent of superficial exposed O2 atoms and the higher concentration of phenol molecules in TN. The influence of the surface coordination species on the optical absorption of TN was analyzed by UV–vis DRS. As shown in Figure 16, the TN can only respond to
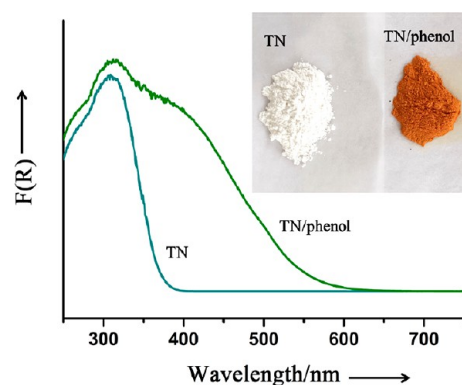

Figure 16. UV–vis DRS of TN and TN/phenol.

the UV light ($\lambda \leq 350$ nm). After the absorption of phenol, the TN shows the visible light absorption property. Accordingly the color of the monolayer TN sample changes from white to yellow after the adsorption of phenol molecules. This result suggests that a ligand-to-metal charge transfer (LMCT) takes place in the surface coordination species, resulting in the

activation of phenol molecules under visible light irradiation.[43] Therefore, the photocatalytic activity of Pd/TN improved from 21% conv. to 25% conv (Table 1, entry 1). Under visible light irradiation, this may be attributed to the enhanced photoabsorption performance and the charge transfer from phenol molecules to TN in the surface coordination species.[42]

To further elucidate the roles of the generated V_O in this phenol hydrogenation reaction, DFT calculations were carried out to study the adsorption behaviors of phenol on the V_O. Considering the Ti vacancies, there are two types of defect oxygen atoms in TN: the defect oxygen adjacent to Ti vacancy (denoted as V_{O1}) and the defect oxygen neighboring perfect TiO_6 octahedron (denoted as V_{O2}). Two computational models of the TN were proposed: V_{O1} and V_{O2}. As shown in Figure S13, the adsorption energy of phenol and cyclohexanone molecules on the V_{O1} and V_{O2} have been calculated. Once the phenol molecules absorb on the V_O, the H atom in −OH of phenol will leave to the nearby O atoms in TN, resulting in the in situ formation of C═O. Moreover, the adsorption energy of cyclohexanone on the V_{O1} and V_{O2} are 2.98 and 1.55 eV, respectively. In these cases, it is difficult for cyclohexanone molecules to desorb from the TN inhibiting the adsorption cycle of phenol molecules. In addition, in situ ESR experiments showed that the signal of V_O was observed throughout the whole catalytic process (Figure 14), suggesting that the V_O in TN is not covered by adsorbing the phenol or cyclohexanone molecules. Moreover, the high selectivity of cyclohexanone over the Pd/TN may also suggest that the generated V_O does not adsorb the phenol molecules. On the basis of the above ESR and DFT calculations results, it can be speculated that these

Scheme 1. Possible Reaction Mechanism of Phenol Hydrogenation over Pd/TN via the Thermocatalytic Process[a]
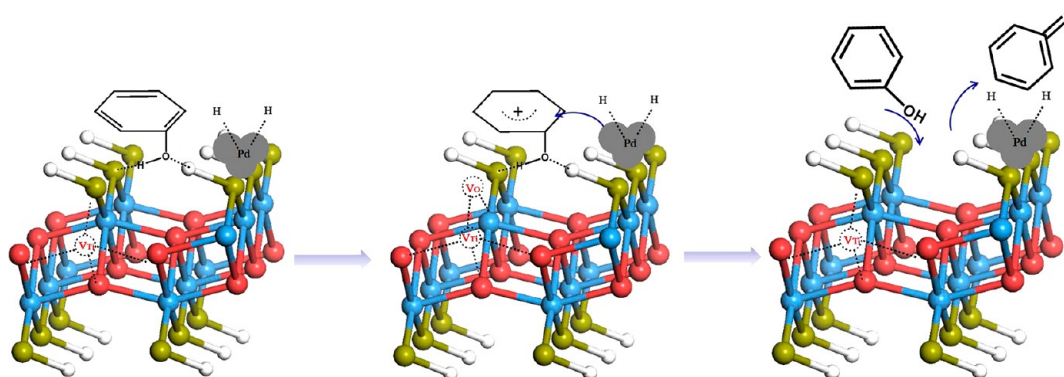

[a]Atoms are color labeled: Ti (blue), H (white), O1 (red), and O2 (yellow).

generated V_O during this reaction might not further adsorb the phenol molecules. However, it is difficult to construct an accurate model of V_O in the experiment. Therefore, the mechanism of the generation for Vo and the role of Vo plays in this reaction is still not fully understood. A further study on Vo will be carried out in the future.

On the basis of the experimental results, the possible catalytic mechanisms for the hydrogenation of phenol to the cyclohexanone over Pd/TN are proposed (Schemes 1 and 2).

Scheme 2. Possible Photo-Promoted Reaction Mechanism of Phenol Hydrogenation over Pd/TN under the Stimulated Irradiation
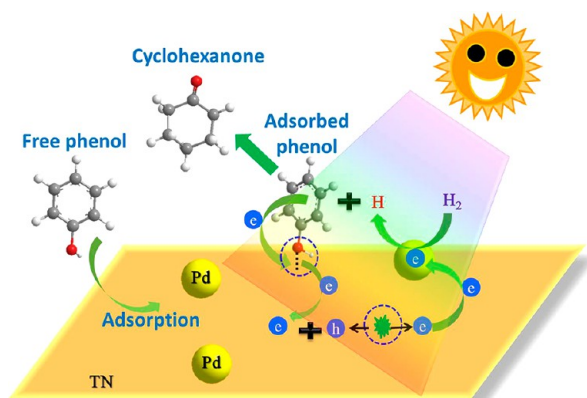
Because of the abundant superficial acid and basic sites in the as-prepared TN, phenol molecules would bind with TN in a nonplanar fashion via a hydrogen-bonding ring forming the surface coordination species. The strong interactions result in the formation of V_O, promoting the exposure of Ti^{4+} (Lewis acid sites). These Lewis acid sites are beneficial to the further activation and hydrogenation of phenol. Under the hydrogen atmosphere, the metallic Pd^0 dissociates hydrogen molecules to form hydrogen atom. Then the activated phenol molecules are hydrogenated by the hydrogen atoms to enol molecules and further transformed to cyclohexanone via a thermocatalytic process (Scheme 1).[1,12] The cyclohexanone is very easily desorbed from the reaction active site on the surface of TN. That is essential for the continuous reaction and avoids further hydrogenation of cyclohexanone to cyclohexanol and cyclohexane.

When the catalytic reaction was performed under the simulated solar light irradiation (Scheme 2), the electron transfer takes place in the surface coordination species from phenol molecules to Pd/TN, resulting in the activation of phenol molecules to produce a carbonium ion. Simultaneously, TN would be excited to generate the electron−hole pairs. Subsequently, the photogenerated electrons transfer to Pd clusters to form electron-rich Pd species and promote the dissociation of molecular H_2 into active H atoms. The photogenerated holes would recombine the photoinduced electron from the surface coordination species. These approaches may be the important reasons for the efficient photocatalytic conversion of phenol over Pd/TN under ambient temperature and pressure. The synergistic effect of the surface coordination species, TN and Pd clusters remarkably facilitate the high yield of cyclohexanone in photocatalysis. Finally, the formed carbonium ion is hydrogenated by the nearby active H in Pd clusters forming an enol intermediate and isomerizes rapidly to cyclohexanone, which is similar to the thermocatalytic process.

The photocatalytic activities of Pd/TN for the hydrogenation of phenol derivatives with a set of substituent groups have also

Table 2. Aqueous-Phase Hydrogenation of Hydroxyl Aromatic Derivatives over the Pd/TN[a]

Entry	Substrate	Time (h)	hv	Conv. (%)	Product	Sel.(%)
1	HO—⟨⟩—OH	10	+	>99	O=⟨⟩—OH	>99
2	HO-/⟨⟩—OH	12	+	>99	(cyclohexanone)	98
3	OH-⟨⟩—OH	12	+	>99	O=⟨⟩—OH	98
4	—⟨⟩—OH	15	+	99	—⟨⟩=O	99
5	⟨⟩—OH	15	+	92	⟨⟩=O	99
6	⟨⟩—OH	15	+	85	⟨⟩=O	97
7	HO—⟨⟩—Cl	8	+	>99	O=⟨⟩	99

[a]Reaction conditions: simulated light irradiation, phenol (0.1 mmol), Pd/$H_{1.07}Ti_{1.73}O_4\cdot H_2O$ 20 mg (Pd 1 wt % relative to $H_{1.07}Ti_{1.73}O_4\cdot H_2O$), water solvent (2 mL), H_2 0.1 MPa unless otherwise noted.

been evaluated. The Pd/TN sample is a widely applicable catalytic system for the hydrogenation of hydroxylated aromatic compounds (Table 2). In all cases, the Pd/TN could catalyze the hydrogenation of phenol derivatives into the corresponding substituted cyclohexanones with high conversion (>99%) and selectivity (>99%). Notably, the substituent groups have affected the reaction rates. Phenol derivatives with electron-donating substituents like $-CH_3$ and $-OH$ show a decreased conversion rate (Table 2, entries 1−6), while a phenol derivative with an electron-withdrawing group like $-Cl$ exhibits a slightly increased conversion rate (Table 2, entry 7). Furthermore, the steric hindrance also affects the reaction rate. The cresol molecules with methyl group ($-CH_3$) at different positions of phenyl ring show the reaction rate in the order of ortho < meta < para. Similar electron and steric hindrance effects were also observed previously over Pd@MMT-1, Pd@mpg-C_3N_4, and Pd-PANI/CNT.[1,2,44]

3. CONCLUSIONS

In summary, the experiments described here demonstrate the feasibility of direct construction of a catalyst for precise synthesis of cyclohexanone using $H_{1.07}Ti_{1.73}O_4 \cdot H_2O$ nanosheets and Pd clusters. This sample exhibits a high conversion (>99%) and high selectivity (>99%) for phenol hydrogenation to cyclohexanone by photocatalysis under ambient temperature and hydrogen atmosphere using water as solvent. These performances are much higher than those of their layered counterparts. The composite catalyst can be also expanded to catalyze the hydroxylated aromatic compounds with high yield. The abundant Lewis acid and basic sites in the surface of monolayer TN were revealed by CO_2-TPD, in situ FTIR, and ^{1}H NMR spectra. These active sites greatly promote the adsorption and activation of phenol molecules by forming the surface coordination species via a hydrogen-bonding ring in a nonplanar fashion. Moreover, the surface highly dispersed negative Pd clusters on the monolayer TN serve as the active sites for the dissociation of H_2 to H atoms. Thus, the activated phenol molecules would react with the strongly reductive H atoms to form enol molecules that further transform to cyclohexanone. Under the simulated solar light irradiation, the photoexcited surface coordination species can induce the surface charge transfer from phenol molecules to TN to form the active carbonium ions. These surface charges may annihilate the photogenerated holes from TN, promoting the separation efficiency of photogenerate electron−hole pairs on TN. Simultaneously, the photogenerate electrons of TN would transfer to the surface Pd clusters for the dissociation of H_2 to H atoms. Finally, this surface synergetic catalytic mechanism would contribute to the high yield of cyclohexanone over Pd/TN. This study not only offers an in-depth fundamental understanding of the photocatalytic mechanism for hydrogenation of phenol at the molecular level but also suggests that these monolayer nanosheets with inherent defects may have great potential in the construction of catalysts for precise organic synthesis.

ASSOCIATED CONTENT

Ⓢ Supporting Information

The Supporting Information is available free of charge on the ACS Publications website at DOI: 10.1021/acscatal.7b03463.

Experimental procedures, preparation and character-ization of catalysts, theoretical calculations method, and cyclic data (PDF)

AUTHOR INFORMATION

Corresponding Authors
*E-mail: sjliang2011@gmail.com (S. Liang).
*E-mail: slin@fzu.edu.cn (S. Lin).
*E-mail: wuling@fzu.edu.cn (L. Wu).

ORCID Ⓘ
Shijing Liang: 0000-0001-9963-5935
Jinhong Bi: 0000-0002-8141-7742
Sen Lin: 0000-0002-2288-5415
Ling Wu: 0000-0003-2652-8105

Notes
The authors declare no competing financial interest.

REFERENCES

(1) Wang, Y.; Yao, J.; Li, H.; Su, D. S.; Antonietti, M. J. *J. Am. Chem. Soc.* **2011**, *133*, 2362−2365.
(2) Lin, C. J.; Huang, S. H.; Lai, N. C.; Yang, C. M. *ACS Catal.* **2015**, *5*, 4121−4129.
(3) Liu, H. L.; Li, Y. W.; Luque, R.; Jiang, H. F. *Adv. Synth. Catal.* **2011**, *353*, 3107−3113.
(4) Mahata, N.; Vishwanathan, V. J. *J. Catal.* **2000**, *196*, 262−270.
(5) Cirtiu, C. M.; Dunlop-Briére, A. F.; Moores, A. *Green Chem.* **2011**, *13*, 288−291.
(6) Zhu, J. F.; Tao, G. H.; Liu, H. Y.; He, L.; Sun, Q. H.; Liu, H. C. *Green Chem.* **2014**, *16*, 2664−2669.
(7) Cheng, H. Y.; Liu, R. X.; Wang, Q.; Wu, C. Y.; Yu, Y. C.; Zhao, F. Y. *New J. Chem.* **2012**, *36*, 1085−1090.
(8) Zhang, D. M.; Guan, Y. J.; Hensen, E. J. M.; Chen, L.; Wang, Y. M. *Catal. Commun.* **2013**, *41*, 47−51.
(9) (a) Li, H.; Liu, J.; Xie, S.; Qiao, M.; Dai, W.; Lu, Y.; Li, H. *Adv. Funct. Mater.* **2008**, *18*, 3235−3241. (b) Ohta, H.; Yamamoto, K.; Hayashi, M.; Hamasaka, G.; Uozumi, Y.; Watanabe, Y. *Chem. Commun.* **2015**, *51*, 17000−17003. (c) Chen, J.; Zhang, W.; Chen, L.; Ma, L.; Gao, H.; Wang, T. *ChemPlusChem* **2013**, *78*, 142−148.
(10) (a) Chatterjee, M.; Kawanami, H.; Sato, M.; Chatterjee, A.; Yokoyama, T.; Suzuki, T. *Adv. Synth. Catal.* **2009**, *351*, 1912−1924. (b) McManus, I.; Daly, H.; Thompson, J. M.; Connor, E.; Hardacre, C.; Wilkinson, S. K.; Sedaie Bonab, N.; ten Dam, J. T.; Simmons, M. J. H.; Stitt, E. H.; D'Agostino, C.; McGregor, J.; Gladden, L. F.; Delgado, J. J. *J. Catal.* **2015**, *330*, 344−353. (c) Zhang, D.; Ye, F.; Xue, T.; Guan, Y.; Wang, Y. *Catal. Today* **2014**, *234*, 133−138.
(11) (a) Morales, J.; Hutcheson, R.; Noradoun, C.; Cheng, I. F. *Ind. Eng. Chem. Res.* **2002**, *41*, 3071−3074. (b) He, J.; Zhao, C.; Lercher, J. A. *J. Catal.* **2014**, *309*, 362−375.
(12) Liu, H.; Jiang, T.; Han, B.; Liang, S.; Zhou, Y. *Science* **2009**, *326*, 1250−1252.
(13) (a) Zhong, J. W.; Chen, J. Z.; Chen, L. *Catal. Sci. Technol.* **2014**, *4*, 3555−3569. (b) Shin, J. Y.; Jung, D. J.; Lee, S. *ACS Catal.* **2013**, *3*, 525−528.
(14) Velu, S.; Kapoor, M. P.; Inagaki, S.; Suzuki, K. *Appl. Catal., A* **2003**, *245*, 317−331.

(15) Wang, Y.; Zhang, J.; Wang, X.; Antonietti, M.; Li, H. *Angew. Chem., Int. Ed.* **2010**, *49*, 3356−3359.

(16) Sikhwivhilu, L. M.; Coville, N. J.; Naresh, D.; Chary, K. V. R.; Vishwanathan, V. *Appl. Catal., A* **2007**, *324*, 52−61.

(17) Zhuang, L.; Li, H. X.; Dai, W. L.; Qiao, M. H. *Chem. Lett.* **2003**, *32*, 1072−1073.

(18) Li, H.; Liu, J. L.; Li, H. X. *Mater. Lett.* **2008**, *62*, 297−300.

(19) Huang, X.; Zeng, Z. Y.; Bao, S. Y.; Wang, M. F.; Qi, X. Y.; Fan, Z. X.; Zhang, H. *Nat. Commun.* **2013**, *4*, 1444.

(20) Tan, C. L.; Zhang, H. *Chem. Soc. Rev.* **2015**, *44*, 2713−2731.

(21) Lu, Y. Z.; Jiang, Y. Y.; Gao, X. H.; Wang, X. D.; Chen, W. J. *J. Am. Chem. Soc.* **2014**, *136*, 11687−11697.

(22) Yang, S. B.; Feng, X. L.; Wang, L.; Tang, K.; Maier, J.; Mullen, K. *Angew. Chem., Int. Ed.* **2010**, *49*, 4795−4799.

(23) Chhowalla, M.; Shin, H. S.; Eda, G.; Li, L. J.; Loh, K. P.; Zhang, H. *Nat. Chem.* **2013**, *5*, 263−275.

(24) Nakajima, K.; Baba, Y.; Noma, R.; Kitano, M.; Kondo, J. N.; Hayashi, S.; Hara, M. J. *J. Am. Chem. Soc.* **2011**, *133*, 4224−4227.

(25) Sun, Y. F.; Gao, S.; Lei, F. C.; Xie, Y. *Chem. Soc. Rev.* **2015**, *44*, 623−636.

(26) (a) Wang, Q.; Zhang, M.; Chen, C. C.; Ma, W. H.; Zhao, J. C. *Angew. Chem.* **2010**, *122*, 8148. (b) Liang, S. J.; Wen, L. R.; Lin, S.; Bi, J. H.; Feng, P.; Fu, X. Z.; Wu, L. *Angew. Chem., Int. Ed.* **2014**, *53*, 2951−2955. (c) Nakajima, K.; Baba, Y.; Noma, R.; Kitano, M.; Kondo, J. N.; Hayashi, S.; Hara, M. J. *J. Am. Chem. Soc.* **2011**, *133*, 4224−4227.

(27) Osada, M.; Sasaki, T. *Adv. Mater.* **2012**, *24*, 210−228.

(28) Sasaki, T.; Ebina, Y.; Kitami, Y.; Watanabe, M. J.; Oikawa, T. *J. Phys. Chem. B* **2001**, *105*, 6116−6121.

(29) Sasaki, T.; Kooli, F.; Iida, M.; Michiue, Y.; Takenouchi, S.; Yajima, Y.; Izumi, F.; Chakoumakos, B. C.; Watanabe, M. *Chem. Mater.* **1998**, *10*, 4123−4128.

(30) Gao, T.; Fjellvåg, H.; Norby, P. J. *J. Phys. Chem. B* **2008**, *112*, 9400−9405.

(31) Sasaki, T.; Watanabe, M.; Hashizume, H.; Yamada, H.; Nakazawa, H. J. *J. Am. Chem. Soc.* **1996**, *118*, 8329−8335.

(32) Maluangnont, T.; Matsuba, K.; Geng, F. X.; Ma, R. Z.; Yamauchi, Y.; Sasaki, T. *Chem. Mater.* **2013**, *25*, 3137−3146.

(33) Ohta, H.; Yamamoto, K.; Hayashi, M.; Hamasaka, G.; Uozumi, Y.; Watanabe, Y. *Chem. Commun.* **2015**, *51*, 17000−17003.

(34) Honda, M.; Oaki, Y.; Imai, H. *Chem. Mater.* **2014**, *26*, 3579−3585.

(35) Xu, Q.; Ma, Y.; Zhang, J.; Wang, X.; Feng, Z.; Li, C. J. *J. Catal.* **2011**, *278*, 329−335.

(36) Takagaki, A.; Sugisawa, M.; Lu, D.; Kondo, J. N.; Hara, M.; Domen, K.; Hayashi, S. J. *J. Am. Chem. Soc.* **2003**, *125*, 5479−5485.

(37) Takagaki, A.; Yoshida, T.; Lu, D.; Kondo, J. N.; Hara, M.; Domen, K.; Hayashi, S. J. *J. Phys. Chem. B* **2004**, *108*, 11549−11555.

(38) (a) Mino, L.; Zecchina, A.; Martra, G.; Rossi, A. M.; Spoto, G. *Appl. Catal., B* **2016**, *196*, 135−141. (b) Turki, A.; Guillard, C.; Dappozze, F.; Ksibi, Z.; Berhault, G.; Kochkar, H. *Appl. Catal., B* **2015**, *163*, 404−414.

(39) (a) Liu, P. X.; Qin, R. X.; Fu, G.; Zheng, N. F. J. *J. Am. Chem. Soc.* **2017**, *139*, 2122−2131. (b) Mu, R.; Zhao, Z. J.; Dohnalek, Z.; Gong, J. L. *Chem. Soc. Rev.* **2017**, *46*, 1785−1806. (c) Gao, C.; Wang, J.; Xu, H. X.; Xiong, Y. J. *Chem. Soc. Rev.* **2017**, *46*, 2799−2823. (d) Moser, J.; Punchihewa, S.; Infelta, P. P.; Graetzel, M. *Langmuir* **1991**, *7*, 3012.

(40) Valenti, G.; Boni, A.; Melchionna, M.; Cargnello, M.; Nasi, L.; Bertoni, G.; Gorte, R. J.; Marcaccio, M.; Rapino, S.; Bonchio, M.; Fornasiero, P.; Prato, M.; Paolucci, F. *Nat. Commun.* **2016**, *7*, 13549.

(41) (a) Alharbi, K.; Kozhevnikova, F.; Kozhevnikov, V. *Appl. Catal., A* **2015**, *504*, 457−462. (b) Amorim, C.; Keane, M. A. *J. Colloid Interface Sci.* **2008**, *322*, 196−208. (c) Pazmino, J. H.; Bai, C.; Miller, J. T.; Ribeiro, F. H.; Delgass, W. N. *Catal. Lett.* **2013**, *143*, 1098−1107. (d) Cargnello, M.; Montini, T.; Polizzi, S.; Wieder, N. L.; Gorte, R. J.; Graziani, M.; Fornasiero, P. *Dalton Trans.* **2010**, *39*, 2122−2127.

(42) (a) Kamegawa, T.; Seto, H.; Matsuura, S.; Yamashita, H. *ACS Appl. Mater. Interfaces* **2012**, *4*, 6635−6639. (b) Zhang, G.; Kim, G.; Choi, W. *Energy Environ. Sci.* **2014**, *7*, 954−966. (c) Yamamoto, Y.; Oaki, Y.; Imai, H. *Adv. Mater. Interfaces* **2017**, *4*, 1601014.

(43) (a) Tae, E. L.; Lee, S. H.; Lee, J. K.; Yoo, S. S.; Kang, E. J.; Yoon, K. B. J. *J. Phys. Chem. B* **2005**, *109*, 22513−22522. (b) Notestein, J. M.; Iglesia, E.; Katz, A. *Chem. Mater.* **2007**, *19*, 4998−5005.

(44) Chen, J. Z.; Zhang, W.; Chen, L. M.; Ma, L. L.; Gao, H.; Wang, T. J. *ChemPlusChem* **2013**, *78*, 142−148.